JOINT EUROPEAN TORUS JET

JET–P(86)43

H.P. Summers, K.H. Behringer and B Denne

Recombination and Population Structure

Recombination and Population Structure

H.P. Summers[1], K.H. Behringer and B Denne

JET-Joint Undertaking, Culham Science Centre, OX14 3DB, Abingdon, UK

[1]Department of Physics, University of Strathclyde, John Anderson Building, 107 Rottenrow, Glasgow G4 0NG, UK

ABSTRACT.

The importance of having reliable estimates of electron-ion recombination coefficients for species such as Ni^{+17} in tokamaks is pointed out. The state of theoretical calculation of recombination rates in thermal plasma is then briefly reviewed.

A new treatment is summarised which unites detailed computation of the direct recombination reactions populating excited ionic energy levels (emphasising dielectronic and radiative recombination) with a careful study of the effects in a plasma of subsequent collisions on the initial direct capture distributions. This includes both singly excited and doubly excited (resonance) state distributions

Illustrations are drawn from fairly ionised ions of interest in laboratory plasmas and include some specific results on recombination of neon-like and adjacent ions of iron, nickel and selenium. these ions either are strongly radiating species in tokamak plasmas such as JET or important X-ray studies

Some results are shown of modelling of nickel ion radiation in JET using the new rate coefficients.

INTRODUCTION

The local densities of ions in a plasma are determined by the balance of ionisation, recombination and diffusion. For an impurity species such as nickel in the JET tokamak, modelling of the ion distribution for a typical pulse incorporating these processes is shown in figure 1. Ni^{+25}, in the central plasma, is determined by the balance between ionisation and recombination, while Ni^{+1} in the edge plasma is determined by the balance between ionisation and inward diffusion. An intermediate ion such as Ni^{+17} is influenced by all three processes. Such intermediate ions are important radiators. Routine measurement of the spatial distribution of spectral radiation from ions such as Ni^{+17} and Ni^{+25} is made on JET. We seek a consistent model from which absolute nickel density and radiated power may be deduced. The impurity diffusion coefficient in JET is inferred empirically to be approximately 1 m^2 sec^{-1} independent of ion charge. This is from the observed positions of radiating shells (eg figure 2). Ionisation and recombination coefficients by contrast are sought from theoretical atomic physics calculation.

For plasma electron densities $N_e \lesssim 10^{14}$ cm^{-3}, an impurity ion is almost certainly in its ground energy level (or lowest metastable level, if present). The effective ionisation coefficient is the ground level, two body electron-ion ionisation rate coefficient and is negligibly dependent on plasma density. The effective recombination coefficient for an ion such as Ni^{+17} at densities $N_e \sim 10^{14}$ cm^{-3} on the other hand is sensitive to density. It is also markedly sensitive to the recombining ion structure. This paper reviews briefly calculations of recombination. A new general calculation for effective recombination coefficients is then described and illustrated. Finally, we return to the modelling of nickel in JET.

2. AN OVERVIEW OF THE RECOMBINATION COEFFICIENT

The effective electron-ion recombination coefficient characterises the growth of the ground level population density of ions A^{+z} due to free electron capture by ions A^{+z+1}. It is a composite coefficient composed of direct electron captures into any accessible energy level of A^{+z} (which is stable to Auger breakup, and called a singly excited state), followed by additional processes which influence or interrupt the captured electron's random walk to the ground level. The relevant direct capture reactions are radiative recombination, dielectronic recombination and three-body recombination. Restricting to electron densities $N_e \lesssim 10^{14}$ cm^{-3} and temperatures T_e at which the ion A^{+z}'s fractional abundance in equilibrium is large, only the first two direct processes are important. The direct dielectronic recombination process is itself a composite process composed of a radiationless transition to a resonant state (the resonant states which are not stable to Auger breakup are called doubly excited) followed by a radiative stabilisation. The doubly excited states can be influenced by additional interactions competing with Auger breakup and radiative stabilisation in finite density plasma. A complete recombination calculation has therefore three steps, namely deduction of direct dielectronic recombination coefficients to singly excited states (including determination of doubly excited state populations), deduction of direct radiative recombination coefficients to singly excited states and deduction of singly excited state populations. In the limit of zero density, only the first and second steps are required since the final effective recombination coefficient is merely the sum of direct captures to all levels. Also, the doubly excited state populations in the first step reduce to simple branching ratio expressions. Most studies have been of these first two steps. An additional layer of complexity is added if consistent inclusion of metastable states is sought. Thus the recombining ion A^{+z+1} may have populated metastable states. The ground and metastable populations of A^{+z} evolve

with comparable time constants but are weakly coupled to each other. Separate effective recombination coefficients are required for each recombined and recombining ion metastable pair. Also in the derivation of the generalised coefficients, there is blurring of the distinction between singly excited and doubly excited states.

Turning firstly to the direct radiative recombination coefficient, table 1 summarises calculations up to about one year ago. The use of hydrogenic formula for capture to whole principal quantum shells and semi intuitive adjustments to them are prominent. There is some use of experimental and refined calculated photoionisation cross-section data for capture to the ground levels. Figure 3 shows some comparisons for the radiative recombination coefficient to Fe^{+23} over all levels. More details are in Summers (1986). From a practical point of view, the large number of states accessible to recombination and the variety of ions precludes the general use of the most sophisticated modern theoretical photoionisation techniques for direct recombination coefficients. For intermediate accuracy results for complex ions, a heirarchy of algorithmic and numerical methods has been established recently (Summers, 1986b; Burgess & Summers, 1987). These use numerical procedures based on observed quantum defects and a variational effective central potential for ground state, metastable state and low angular momentum excited state capture, linked to hydrogenic methods for high angular momentum capture. The specification includes arbitrary LS coupled resolution. The formulation is in terms of a generalisation of bound-free Gaunt factors. Figure 4 shows variation of the bound-free Gaunt factor, g^{II}, with z for recombination to form Na-like states. Figure 5 shows some recombination coefficients to a variety of states of Fe^{+21}. More details are contained in Burgess & Summers (1987).

Turning to a dielectronic recombination, table 2 summarises zero density limit calculations of the dielectronic coefficient up to about one year ago. Figure 6 shows some

zero density comparative results for Fe^{+20}. These should be viewed in the light of the basic reaction sequence relevant at zero density, namely

$$A^{+z+1}(i) + e \rightleftarrows A^{+z}(j,n\ell) \quad . \quad \rightarrow A^{+z+1}(k) + e$$

$$\quad . \quad A^{+z}(k,n\ell) + h\bar{\nu}$$

$$A^{+z}(i,n\ell) + h\bar{\nu} \quad .$$

Dielectronic recombination . Alternative Auger and radiative branchings

We also draw attention to the seminal part played by the Burgess General Formula (Burgess, 1965). More details are in Summers (1986a). The coefficient is sensitive to the 'parent ion' transition i→j. Distinction is useful between cases when the transiting parent electron between states i and j does not change its principal quantum number ($\Delta n=o$ transitions) and those when it does. For $\Delta n=o$ transitions, the General Formula tends to be quite accurate, and very high n shells are strongly populated. For $\Delta n>o$, the General Formula is less reliable and fairly low n shells are populated. Alternative branchings, if energetically accessible, can cause significant disturbance of the main dielectronic pathway. The outer electron-orbital, $n\ell$, is approximately hydrogenic except when n belongs to, or is close to the set of quantum numbers represented in the parent states i or j. Thus the most relevant considerations for calculation improvement are

(a) The parent ion transition type (the Δn problem)

(b) Capture to the lowest accessible levels (the low level problem)

(c) Competing branching with radiative stabilisation (the alternative branching problem)

(d) Disturbance of the states j, $n\ell$ at finite density by collisions (the doubly-excited state redistribution problem)

We return to the calculation of the direct dielectronic coefficients in the next section. Presupposing these are correctly determined, the effective recombination coefficient (properly called the 'collisional-dielectronic recombination coefficient', α_{cd}) is obtained in the course of solution for the singly-excited populations $A^{+z}(i,n\ell)$. It is density sensitive because of reionisation of such excited states before the $n\ell$ electron reaches the ground level. Figure 7 illustrates the behaviour of α_{cd}.

3. A NEW RECOMBINATION CALCULATION

We have established chained semi-automatic computational procedures for a complete recombination calculation. An initial description has been given by Summers et al (1987) and a full description is to be published elsewhere. Here we wish to illustrate the steps only. The first step is calculation of direct dielectronic recombination coefficients to the lowest accesible levels. For example, in $Se^{+25} + e \rightarrow Se^{+24}$, the initial fluorine-like parent ion term is $2s^22p^5\ ^2P$. Capture is possible into n=3 levels of the form $2s^22p^5\ 3\ell$ and $2s2p^6\ 3\ell$ via doubly excited states $2s^22p^4\ 3\ell'3\ell''$ and $2s2p^5\ 3\ell'3\ell''$ for all ℓ, ℓ', ℓ''. We include all terms of these configurations. The results are shown in figure 8. Auger and spontaneous emission coefficients are computed using a multielectron, multiconfiguration structure code extended to include distorted free waves (Badnell, 1985) and then composed into recombination coefficients automatically. At usual densities, doubly excited (n=3) state redistribution is negligible. The next step is calculation of direct dielectronic recombination coefficients to all higher quantum shells for the captured electron. For example, for $Ni^{+17} + e \rightarrow Ni^{+16}$, the initial parent ion term is $2s^22p^63s\ ^2S$ and possible $\Delta n=0$ parent transitions ($i \rightarrow j$) are $2s^22p^63s$-$2s^22p^63p$ and $2s^22p^63s$-$2s^22p^63d$. The relevant doubly excited states of Ni^{+16} are therefore of the form $2s^22p^63p\ n\ell$ and $2s^22p^63d\ n\ell$. In thermal plasmas, the populations are usually expressed in terms of Saha-Boltzmann deviations

b(j,nℓ) (the b-factors). In the zero density limit these might be expected simply to be branching ratios of the form Aa/(Aa+Ar) and tend to 1 for Aa>>Ar. The b-factors for states $2s^2 2p^6 3p\ n\ell$ which actually result are shown in figure 9. Necessary Auger rates are obtained by firstly calculating threshold partial collision strengths in the distorted wave approximation for the parent excitations and then projecting these below threshold. We include allowed and forbidden excitations. The ℓ-redistribution of doubly excited populations is by positive ion collision. The complete high level solution includes also Δn=1 parent excitations and all alternative branchings. The direct recombination coefficients to levels of the form $2s^2 2p^6 3s\ n$ which result from all the direct processes are shown in figure 10. The last step is the calculation of the singly excited populations and the deduction of α_{cd}. Continuing with the Ni^{+16} illustration, the populations of singly excited states of the form $2s^2 2p^6 3s\ n$ are shown in figure 11 and also the resultant α_{cd}. In presenting these illustrations we have avoided cases with the added complexity of metastables and angular resolution of singly excited state populations. These details are nevertheless amenable to calculation by our computational scheme. More details are contained in Summers et al (1987)

4. THE ABUNDANCE OF NICKEL IN JET

The new recombination rate coefficients for Ni^{+17} and Ni^{+16} described here were incorporated in the transport model used to provide the radial nickel distribution in figure 1. Some further details, including specification of the ionisation rate coefficients, are in Summers et al (1987). Agreement of nickel abundances derived from spectrum lines of different ionisation stages would give added confidence to our transport model and its associated atomic rate coefficient data. The resonance lines of Ni^{+25} and Ni^{+16} are particularly suitable. The helium-like and lithium-like stages are in the near coronal regime and their ionisation

and recombination rate coefficients are amongst the best established. Also they are not strongly density sensitive. The Ni^{+16} stage on the other hand is influenced by transport and its recombination coefficient is density sensitive. Table 3 shows a comparison of nickel abundances from Ni^{+17}, Ni^{+24} and Ni^{+25} lines for a JET pulse and tends to indicate broad agreement. Evidently such results do not provide a definitive test on any single rate coefficient but nonetheless give some encouragement that the theoretical atomic rates are approaching the true values.

REFERENCES

Aldrovandi S M V & Pequingnot D (1973) Astron. & Astrophys. 25, 137

Badnell N R (1985) Cambridge University, Applied Mathematics Dept. Report DAMPT/AA-1J01-NRB

Behringer K H, Denne B, Magyar G, Breton C, De Michelis C, Ramette J, Saoutic B (1986) Proc. Workshop on Basic and Adv. Fusion Plasma Diag. Techniques, Varenna, Italy

Beigman I L, Vainshtein L A and Chickov B N (1981) Sov. Phys. JETP 53, 490

Barfield W P (1975) Nucl. Fusion 15, 1192

Barfield W P (1979) Astrophys. J. 229, 856

Bely-Dubau F, Gabriel A H and Volonte S (1979) Mon. Not. R. Astr. Soc. 186, 405

Burgess A (196) Mem. R. Astr. Soc. 69, 1

Burgess A (1965) Astrophys. J. 141, 1588

Burgess A & Chidichimo M C (1983) Mon. Not. R. Astr. Soc. 203, 1269

Burgess A & Seaton M J (1960) Mon. Not. R. Astr. Soc. 120, 121

Burgess A & Summers H P (1976) Mon. Not. R. Astr. Soc. 174, 345

Burgess A & Summers H P (1987) Mon. Not. R. Astr. Soc. (in press)

Burgess A & Tworkowski A S (1976) Astrophys. J. 205, L105

Dubau J, Gabriel A H, Loulerque M, Steenman-Clark L & Volonte S (1981) Mon. Not. R. Astr. Soc.195, 705

Hahn Y, Gau J N, Luddy R & Retter J A (1980) J. Quant. Spect. Rad. Transf. 23, 65

Jacobs V L, Davies J, Kepple P C, Blaha M (1977) Astrophys. J. 211, 305

Lee C M & Pratt R H (1975) Phys. Rev. A12, 1825

Mertz A L, Cowan R D & Magee N H (1976) Los Alamos Report LA-6620-175

Peach G (1967) Mem. R. Astr. Soc. 71, 13

Post D E, Jensen R V, Tarter C B, Grasberger W H, Lokke W A (1977) At. Data Nucl. Data Tables 20, 397

Safronova U I (1975) J. Quant. Spect. Rad. Transp. 15, 231

Seaton M J (1959) Mon. Not. R. Astr. Soc.119, 81

Seaton M J (1964) Planet Space Sci. 12, 55

Seaton M J & Storey P J (1976) "Atomic Processes & Applications" - ed. Burke & Moiseiwitsch - North Holland

Shore B (1969) Astrophys. J. 158, 1205

Summers H P (1986a) JET Joint Undertaking report JET-IR(86)01

Summers H P (1986b) JET Joint Undertaking report JET-P(86)06

Summers H P, Behringer K H & Wood L (1987)Physics Scripta (in press)

Tartar C B (1971) Astrophys. J. 168, 313

Tartar C B (1973) Astrophys. J. 181, 607

Von Goeler (1975) Nucl. Fusion 15, 301

Table 1. Summary of radiative recombination calculations.

		Authors	Seaton 1959	Burgess & Seaton 1960	Seaton 1964	Burgess 1964	Peach 1967	Tarter 1971 1972	Aldrovandi & Pequignot 1973	Von Goeler 1975	Lee & Pratt 1975	Burgess & Summers 1976	Gould 1978	Barfield 1979 1975
hydrogenic ion	ground state	adjust.						ionisation potential + weight		ionisation potential + weight			ionisation potential + weight	
		resol.	n			nl		n	"	n		n	n	
		comment						used for general ions excluding specific cases below		formula			formula based on specific calculations below	
	excited state	resol.	n			nl		n	n	n		n	n	nl
		comment	uses asymptotic g^{II} α_n formulae			exact g^{II}'s and α_{nl}'s $n<20$ numerical		$g^{II}=1$ formula	uses Seaton 1959 formula	$g^{II}=1$ formula		improved g^{II} formula	modified hydrogenic as for ground state	$l>n$
complex ion	ground state	resol.		arbitrary			arbitrary	nl	nl				nl	nl
		comment		correct fractional parentage g^{II} formulae			correct fractional parentage g^{II} formulae + numerical	experimental $a_{\vec{p}}$ used for some specific ions	experimental $a_{\vec{p}}$ used for some specific ions. extensive sq. extrapol.				experimental threshold $a_{\vec{p}}$ used for some specific ions	central potential model numerical
	excited state	resol.		arbitrary			arbitrary							nl
		comment		$n\leq 12$ $l\leq 3$ g^{II} formula			$n\leq 12$ $l\leq 3$ g^{II} formulae + numerical							$l<n$ as above numerical
Total rate			α_{tot} formula		α_{tot} formula			α_{RR} formula						
comments				needs μ's, δ's and numerical quadrature quantum defect method	applies at peak abundance temperature		needs μ's, δ's and numerical quadrature quantum defect method	detailed results for H, C-C^{+3} N-N^{+2}, O-O^{+3} Ne-Ne^{+5} $Mg-Mg^{+7}$	detailed results for C, N, O, Ne Mg, Si, S ions extrapolation for ion charge >4		applied to high energy electron capture only.	numerical quadrature	detailed results for C-C^{+3}, N-N^{+3} O-O^{+3}, Ne-Ne^{+3} $Mg-Mg^{+3}$, Si-Si^{+3} S-S^{+3}, Ar-Ar^{+3}	lithium-like sequence $n\leq 6$ (1979) iron ion results (1975

Table 2. Summary of dielectronic recombination calculations.

	Authors	Burgess 1965	Shore 1969	Seaton + Storey 1976	Burgess + Tworkowski 1976	Merts, Cowan + Magee 1976	Jacobs et al. 1977	Bely-Dubau et al. 1979, 1982	Dubau et al. 1981	Beigman et al. 1981	Hahn + Coworkers 1980, ...	Safronova + coworkers 1975, ...	Younger 1983
Method		correspondence principle + program + general formula	screened Coulomb orbitals	UCL distorted wave codes + correspondence principle approach	screened Coulomb orbitals multiconfig.	central field orbitals multistate multiconfig.	distorted wave codes + correspondence principle approach.	UCL codes Thomas-Fermi-Dirac orbitals. multiconfig.	UCL codes Thomas-Fermi-Dirac orbitals multiconfig	correspondence principle approach + Coulomb-Born semi empirical	Hartree-Fock orbitals	Z-expansion	frozen core Hartree-Fock orbitals.
doubly excited states	coupling scheme	no coupling	no coupling	LS + pair studied	$_{S}LS$	no coupling discussed	no coupling	LSJ	LSJ	no coupling	no coupling	LSJ	LS
	Auger rate averaging	nl resolution	nl resolution	investigated	LS resolution	nl resolution discussed	nl resolution	LSJ	LSJ	nl resolution	nl resolution	LSJ	LS resolution
	alternate Auger channels	yes	no	no	no	no ? discussed	yes	yes ?	yes ?	yes	yes & cascade correction	no.	no
	highest explicit levels		$n=10$		$n=5$	$n=5$ in general		$n=4$	$n=4$		$n=5$	$n=4$	$n=7$ $\ell \leq 3$
	method of projection	downward from continuum	extrapolation of Slater integrals	downward from continuum	n^{-3}	$n^{-3}\ell^{-\beta}$ for some β	downward from continuum	n^{-3} improved	n^{-3} improved	downward from continuum	n^{-3} improved	none	n^{-3}
	Comment				low Z adjustments								$1s2p(^3P)n\ell - 1s^2n\ell$ stabilisation allowed
initial and final ions	metastable initial states	no	no.	no	no	yes - in ground config. only. statistical.	no	no	no	no	no	no	no
	resolved α given	available in program	easily obtained	easily obtained	available but not published	easily obtained	no	not explicit but available	not explicit but available	no	not explicit	not explicit	no
	α_{tot} given	general formula	yes	yes	as correction & general formula	yes for Fe^{+21}, Fe^{+22}	composite (radiative + dielectronic)	yes	yes	yes	yes	no	yes
	ions treated	any	H-like, Li-like Na-like, K-like B-like ($Z \leq 7$) Capturing ions	Fe^{+21} capturing ion and others	H-like capturing ions	Fe^{+25}, Fe^{+24}, Fe^{+23} Fe^{+22}, Fe^{+21}, Fe^{+20} F^{+9}, Fe^{+15} capturing ions	$Fe^{+25} - Fe^{+8}$ capturing ions papers on other elements	He-like capturing ions including Fe^{+24}	H-like capturing ions including Fe^{+25}	$Fe^{+25} - Fe^{+19}$ $O^{+7} - O^{+1}$ capturing ions	He-like, Li-like Be-like, Na-like Ne-like capturing ions of Ar, Fe, Mo	initial configs. of form $1s^2 2s^p 2p^q$	He-like capturing ions C^{+4}, At^{+11} At^{+14} Fe^{+24}
	Comment												
Comments		program includes correction factors to improve projection. general formula incorporates representative corrections	theoretical paper discussing coupling schemes. Execution errors give false results. Comments on general formula incorrect.	theoretical paper assessing methods + commenting on the general formula.		extensive discussion. focusses on inner core electron excit. mostly so incomplete for usual α_{tot}.	gives (radiative + general formula) comparative values	comparison with general formula is misleading	comparison with general formula is misleading	comparisons with other methods. temperature correction is needed to α_{tot}.		concerned with satellite lines in the vicinity of the 1s-2p resonance line only.	gives comparison with general formula but uses hydrogenic f's and energies

TABLE 3

Comparison of nickel densities derived from various ions JET pulse 4831 at 6·5 secs.

ION	B-C/B-M (cm^{-3})	Present (cm^{-3})
Ni^{+17}	$6 \cdot 4^{10}$	$3 \cdot 9^{10}$
Ni^{+24}	$2 \cdot 2^{10}$	
Ni^{+25}	$3 \cdot 0^{10}$	

B-C/B-M denotes the Burgess-Chidichimo (1983) ionisation sites and the Burgess General Formula (1965) for dielectronic recombination, modified by the prescription of Mertz et al. (1976) for $\Delta n=1$ and adjusted for density following Post et al. (1977).

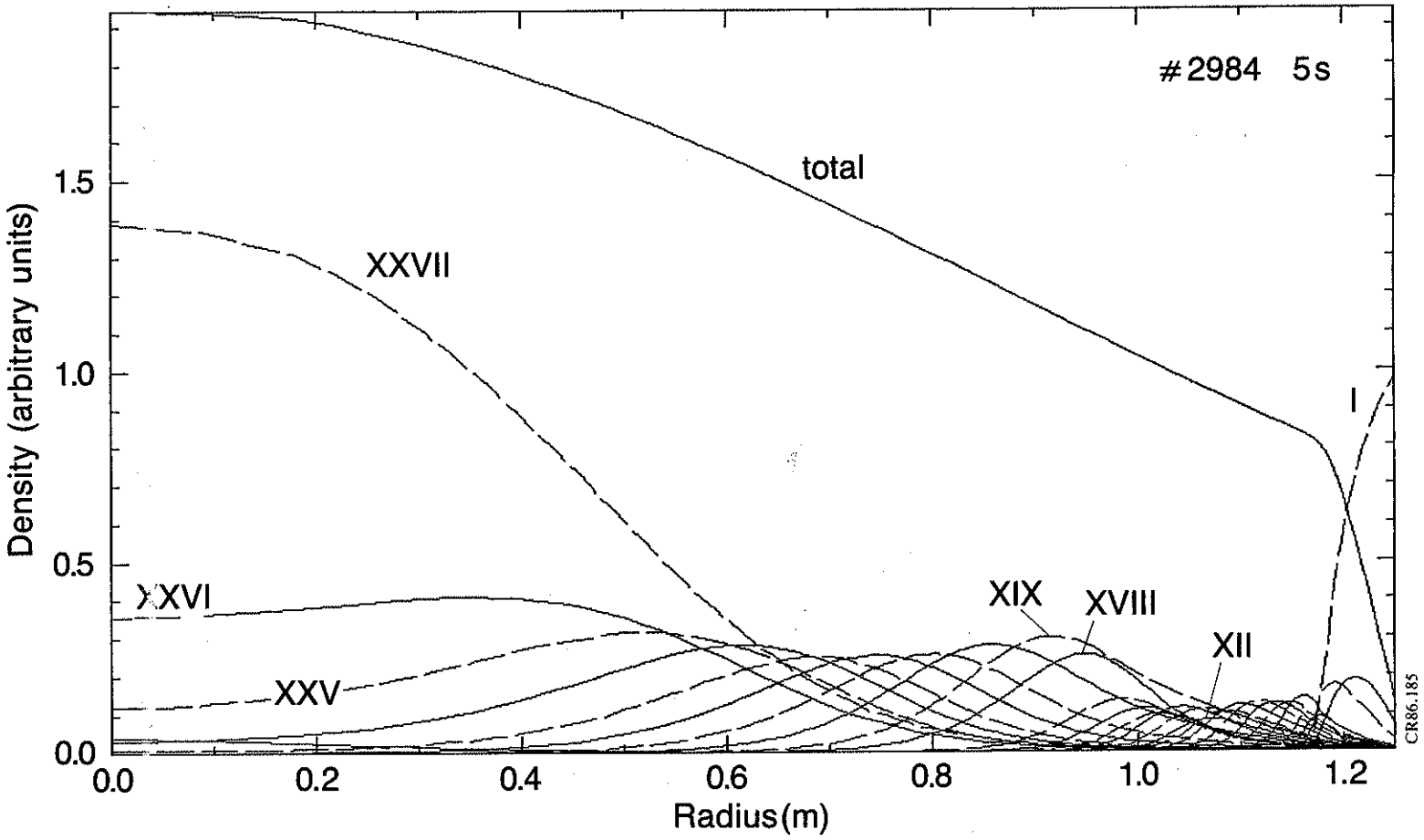

Fig. 1 Distribution of nickel ion densities radially in a JET discharge determined from an impurity transport code.

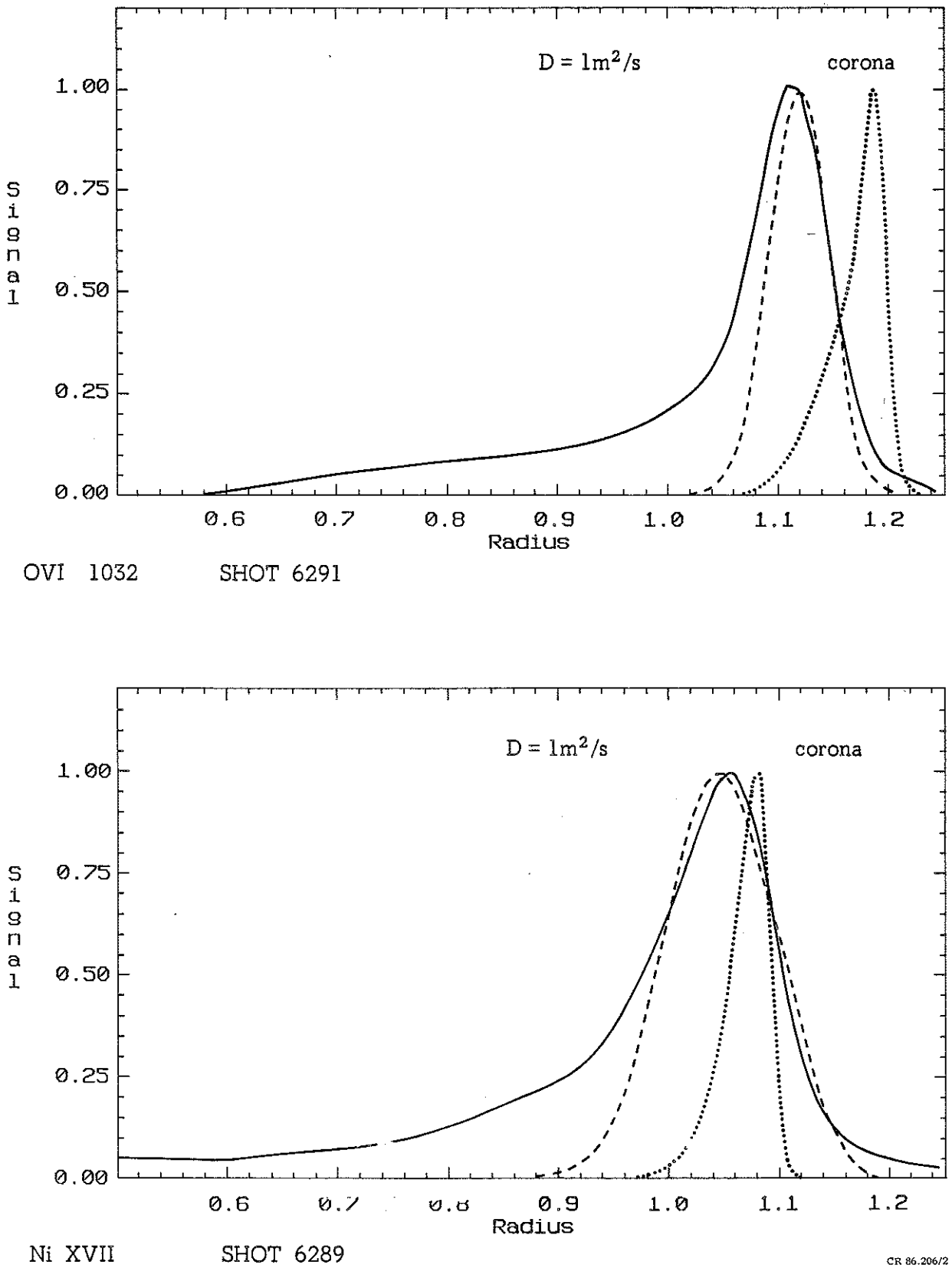

Fig. 2 Abel-inverted profiles and transport code predicted ones in JET discharges.
_____ Abel inverted measured profile; _ _ _ _ transport code predicted profile;
. . . . . coronal model profile (see Behringer et al, 1986).

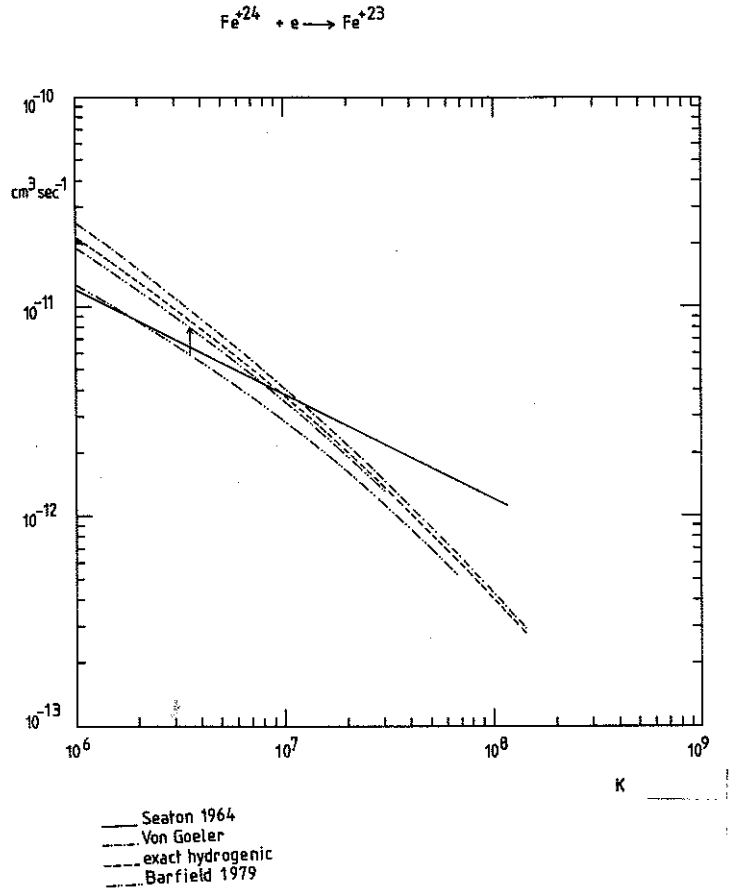

Fig. 3 Comparison of net radiative recombination coefficients for $Fe^{+24} + e \rightarrow Fe^{+23}$. The data of Barfield includes levels up to $n = 6$. This gives the lower curve. It has been corrected upwards by including the exact hydrogenic values for higher n's.

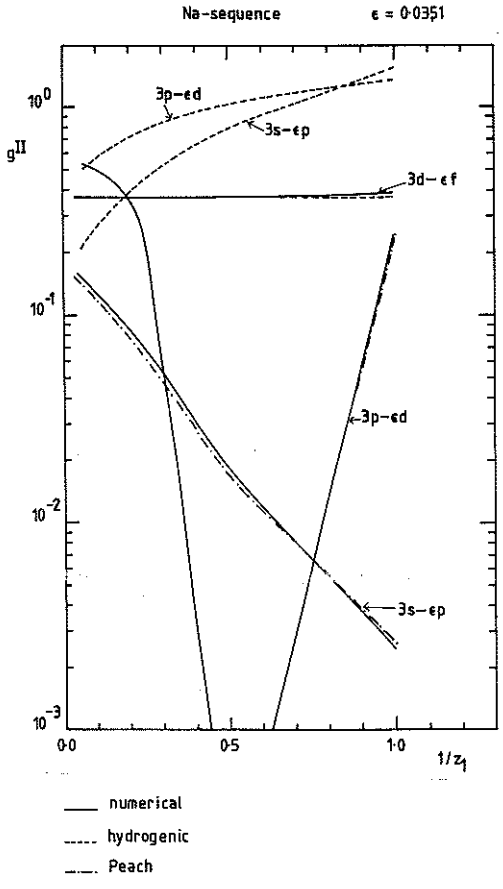

Fig. 4 Variation of the bound-free Gaunt factor (g^{II}) with ion charge for the Na-sequence. z_1 is the recombining ion charge. ϵ is the reduced free electron energy (Summers, 1986b).

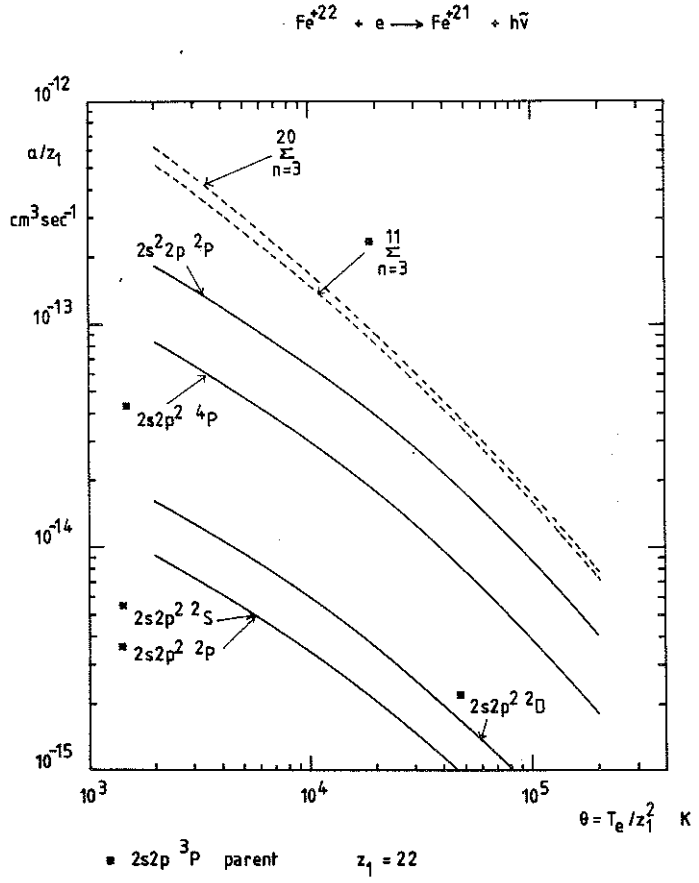

Fig. 5 Scaled radiative recombination coefficients to selected levels for $Fe^{+22} + e \rightarrow Fe^{+21}$. z_1 is the recombining ion charge. θ is the reduced electron temperature.

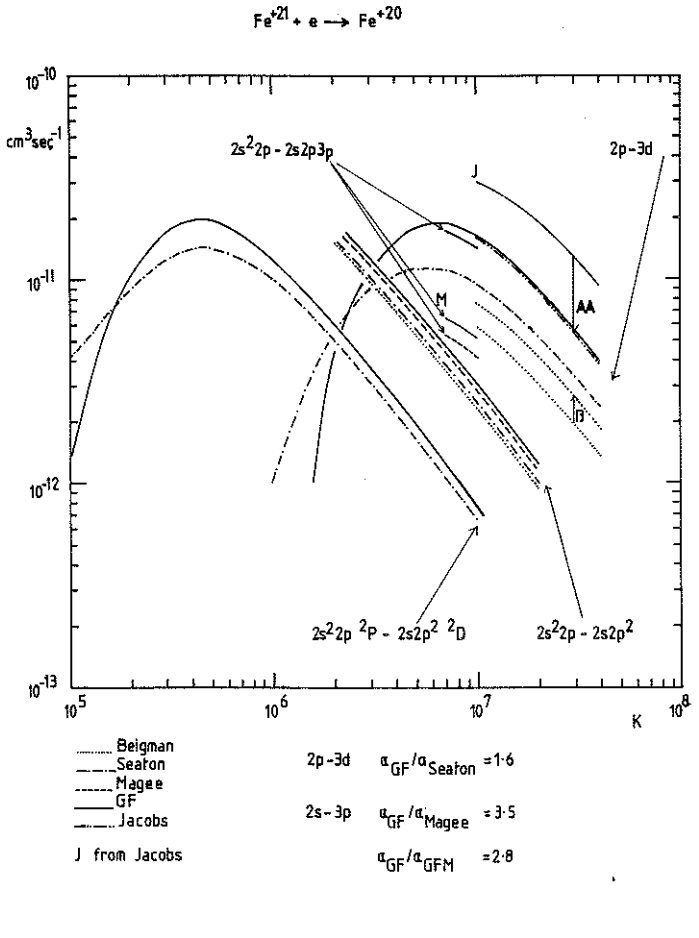

Fig. 6 Comparison of net dielectronic recombination coefficients at zero density for $Fe^{+21} + e \rightarrow Fe^{+20}$ for various core (parent) transitions. Short curves are determined at $T_e = 10^7$ K only. A temperature correction β is made to the results of Beigman (see Summers, 1986b). Seaton and Storey values for the whole core excitation $2s^22p - 2s2p^2$ have been [illegible] by scaling up with oscillator strengths. The Jacobs estimate for α_{GF} for the $2p - 3d$ core excitation is very high. Also, Jacobs shows a large alternative Auger channel correction. Beigman indicates that there is no significant alternative Auger channel correction. The Mertz reduction (Magee et al) is good for the more unusual $\Delta n = 1$ inner shell core excitation but less good for the usual outer shell excitation.

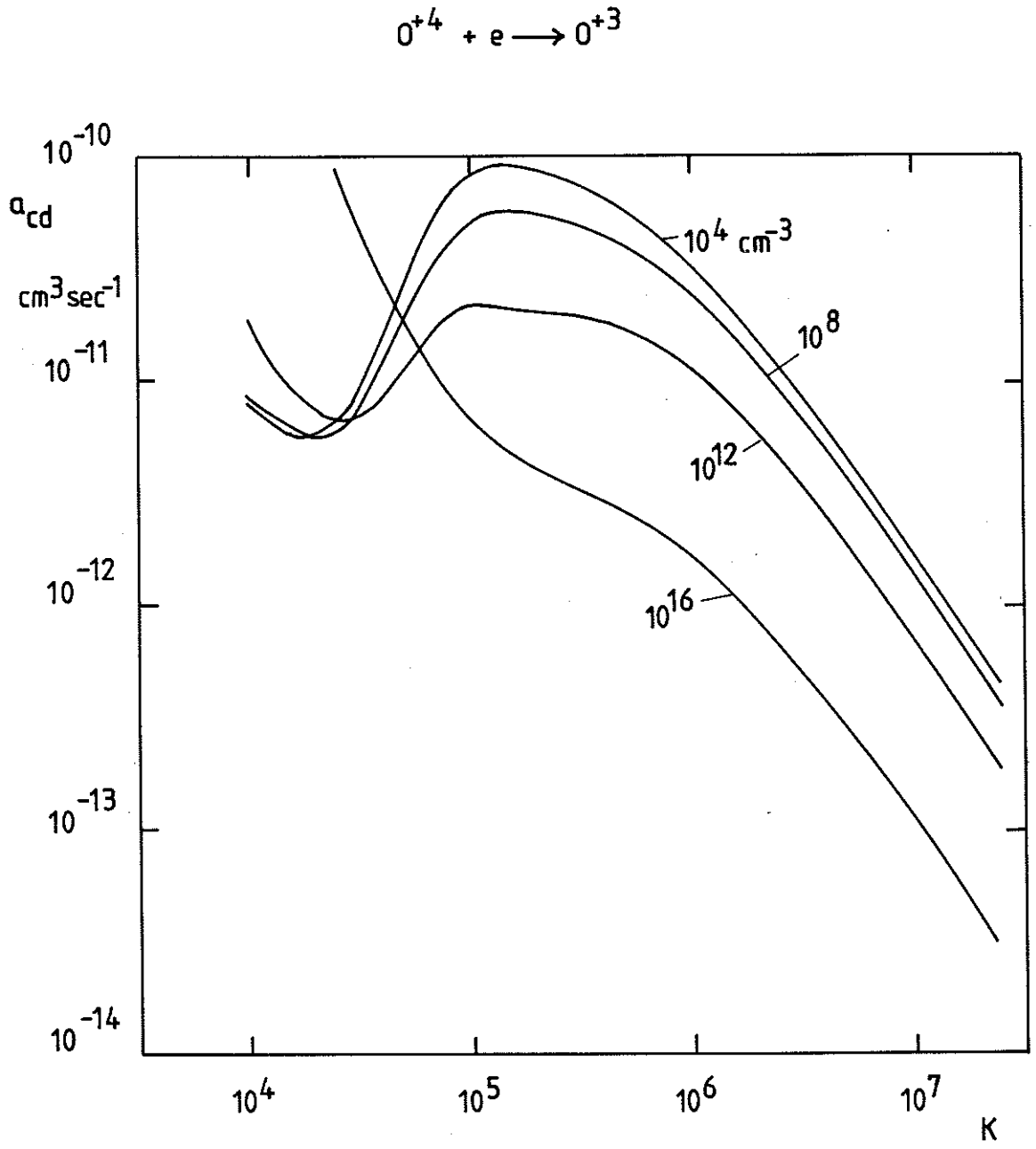

Fig. 7 Variation of collisional-dielectronic recombination coefficients with temperature and density for $O^{+4} + e \rightarrow O^{+3}$.

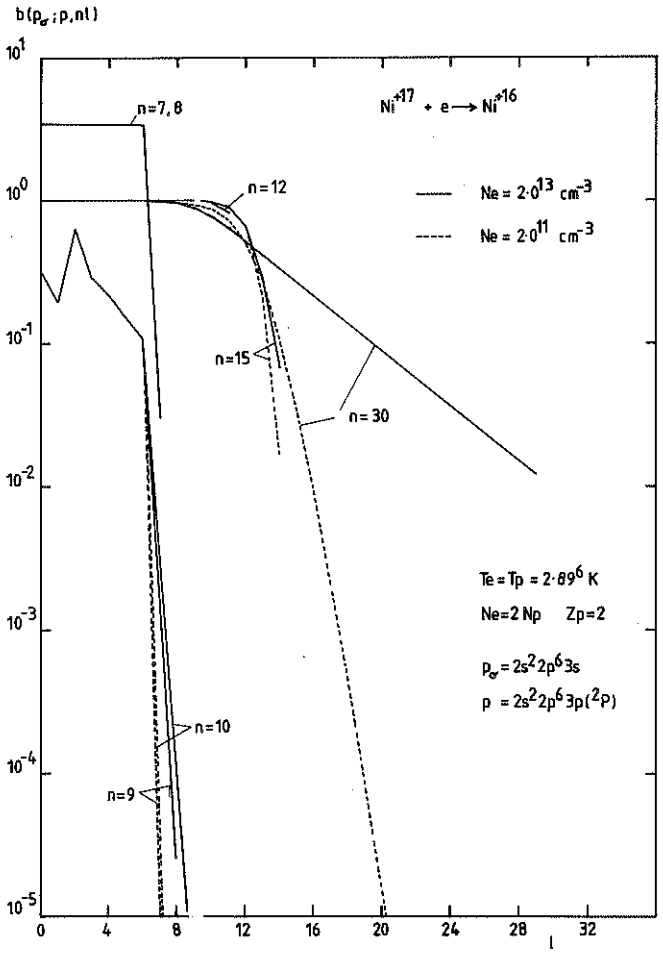

Fig. 9 b-factors for doubly excited states of Ni^{+16}. p_σ is the initial capturing parent ion state, p is the parent state on which the doubly excited states are based. Parent configurations included are $2s^22p^63s$ $2s^22p^63p$ and $2s^22p^63d$.

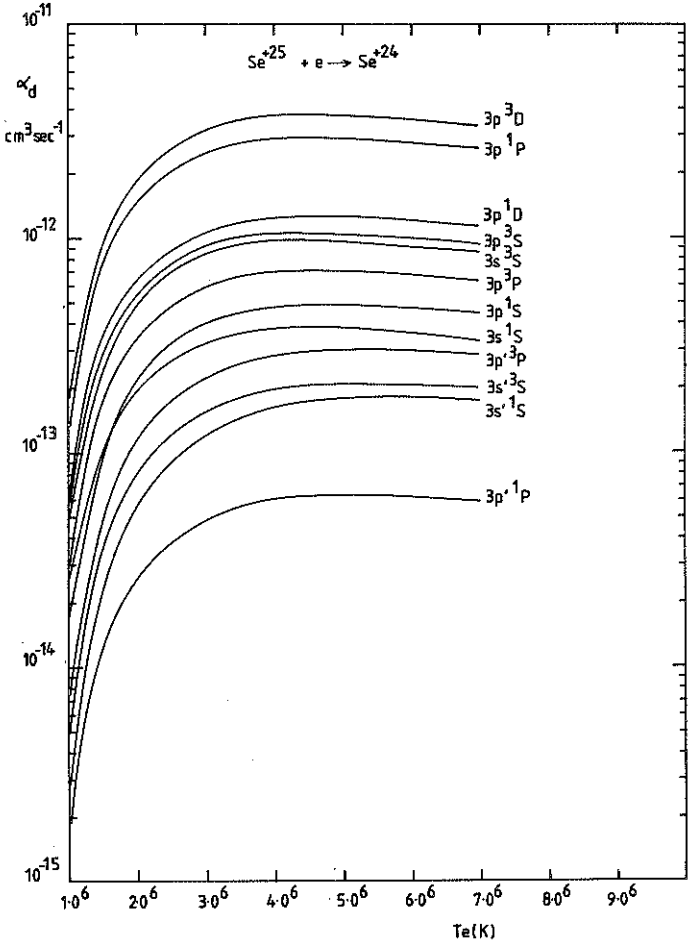

Fig. 8 Direct dielectronic recombination coefficients to selected $n=3$ terms via $n=3$ doubly excited states for $Se^{+25} + e \rightarrow Se^{+24}$. Unprimed terms have $2s^22p^5$ parent, primed terms have $2s2p^6$ parent.

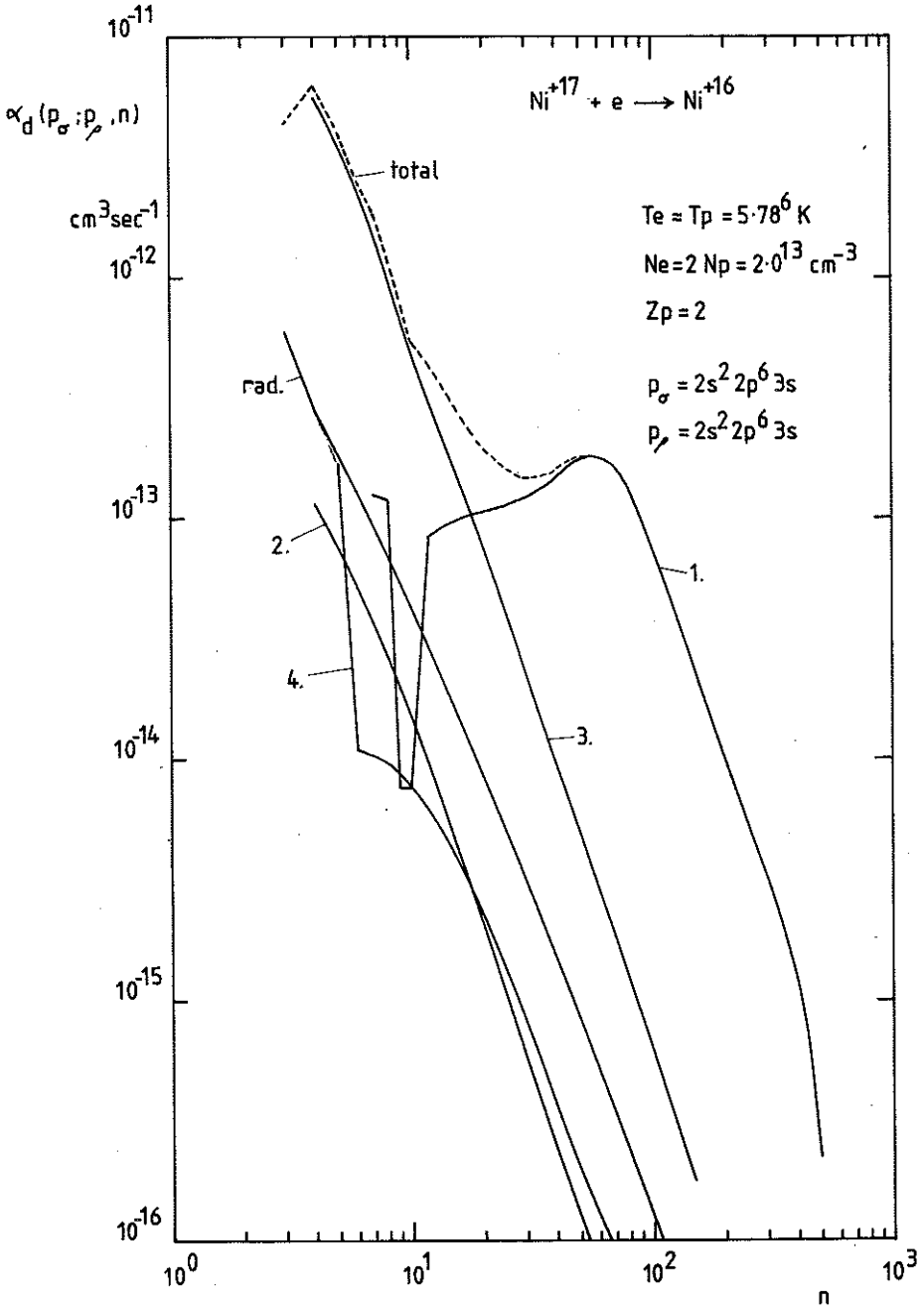

Fig. 10 Direct dielectronic coefficients to n shells for $Ni^{+17} + e \rightarrow Ni^{+16}$. p_σ is the intial capturing parent ion state, p_ρ is the final parent state. Contributions to the total arise from

1. $2s^2 2p^6 3s$, $2s^2 2p^6 3p$, $2s^2 2p^6 3d$
2. $2s^2 2p^6 3s$, $2s^2 2p^5 3s^2$
3. $2s^2 2p^6 3s$, $2s^2 2p^5 3s3d$, $2s^2 2p^5 3s3p$, $2s^2 2p^6 3d$
4. $2s^2 2p^6 3s$, $2s2p^6 3s3p$, $2s^2 2p^5 3s3p$, $2s2p^6 3s^2$

Radiative recombination coefficients are also shown.

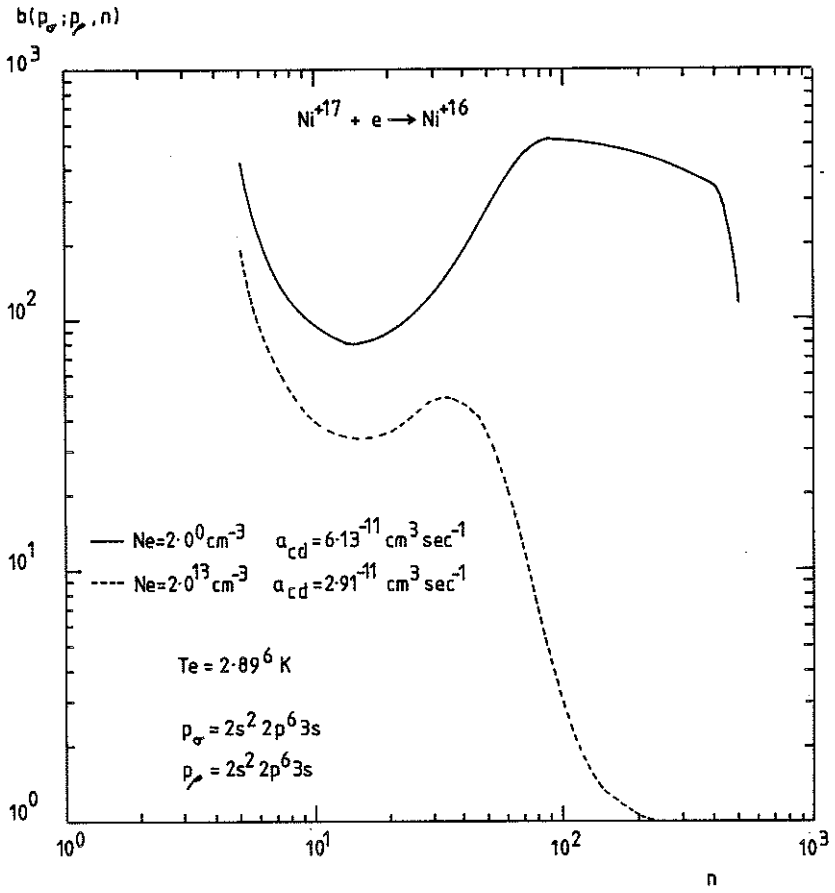

Fig. 11 Singly excited population structure of n shells for Ni^{+16}. α_{cd} is the collisional-dielectronic recombination coefficient.